Journal of Visualized Experiments

Digestion of Whole Mouse Eyes for Multi-Parameter Flow Cytometric Analysis of Mononuclear Phagocytes

--Manuscript Draft--

Article Type:	Invited Methods Article - JoVE Produced Video
Manuscript Number:	JoVE61348R2
Full Title:	Digestion of Whole Mouse Eyes for Multi-Parameter Flow Cytometric Analysis of Mononuclear Phagocytes
Section/Category:	JoVE Immunology and Infection
Keywords:	Eye; Flow Cytometry; Macrophage; microglia; monocyte; Mononuclear Phagocyte; Myeloid
Corresponding Author:	Jeremy A Lavine, MD PhD Northwestern University Chicago, IL UNITED STATES
Corresponding Author's Institution:	Northwestern University
Corresponding Author E-Mail:	jeremy.lavine@northwestern.edu
Order of Authors:	Steven Droho
	Carla M. Cuda
	Jeremy A Lavine, MD PhD
Additional Information:	
Question	**Response**
Please indicate whether this article will be Standard Access or Open Access.	Standard Access (US$2,400)
Please indicate the **city, state/province, and country** where this article will be **filmed**. Please do not use abbreviations.	Chicago, IL, USA

Dear Editorial Board,

I am pleased to resubmit an invited (by Aaron Berard) methods article entitled "Multi-parameter flow cytometic analysis of mononuclear phagocytes from whole mouse eyes" by Steven Droho, Carla M. Cuda, and Jeremy A. Lavine for consideration for publication in *JoVE*.

We have carefully and thoroughly considered the reviewer's criticisms and responded appropriately. We have already completely satisfied Reviewer 1 and Reviewer 2. Reviewer 3 was concerned regarding the lack of systemic perfusion and we have performed an experiment, demonstrating that systemic perfusion is an optional step that did not influence mononuclear phagocyte numbers in the eye with or withour laser injury. We amended Figure 5 to demonstrate our results, both with and without systemic perfusion, to satisfy the reviewer's concern. Additionally, we have satisfied all of Reviewer 4's major and minor concerns, including more detail on microglia, additional citations, and further explanation of our iterative digestion process for optimization of mononuclear phagocytes. Lastly, we have responded to all Editorial comments.

We believe that this manuscript is an excellent fit for JoVE because there are few publications on multi-parameter flow cytometry in mouse eyes. Many ocular researchers still rely on immunofluorescence imaging with IBA-1 alone to identify macrophages and microglia. Furthermore, there are no methods articles on multi-parameter flow cytometry in mouse eyes, and the nuances of the dissection and digestion are best illustrated through videography.

This manuscript has not been published and is not under consideration for publication elsewhere. The principal investigator had full access to all the data in the study and takes responsibility for the integrity of the data and the accuracy of the data analysis as well as the decision to submit for publication. We have no conflicts of interest to disclose.

Thank you for your consideration!

Sincerely,

Jeremy A Lavine, MD PhD
Assistant Professor of Ophthalmology
Northwestern University

TITLE:

Digestion of Whole Mouse Eyes for Multi-Parameter Flow Cytometric Analysis of Mononuclear Phagocytes

AUTHORS AND AFFILIATIONS:

Steven Droho[1], Carla M. Cuda[2*], Jeremy A. Lavine[1*]

[1]Department of Ophthalmology, Feinberg School of Medicine, Northwestern University, Chicago, IL, USA

[2]Department of Medicine, Division of Rheumatology, Feinberg School of Medicine, Northwestern University, Chicago, IL, USA

*These authors contributed equally to the work

Email address of corresponding author:

Jeremy A Lavine (jeremy.lavine@northwestern.edu)

Email address of co-authors:

Steven Droho (steven.droho@northwestern.edu)

Carla M Cuda (c-cuda@northwestern.edu)

KEYWORDS:

eye, flow cytometry, macrophage, microglia, monocyte, myeloid

SUMMARY:

This protocol provides a method to digest whole eyes into a single cell suspension for the purpose of multi-parameter flow cytometric analysis in order to identify specific ocular mononuclear phagocytic populations, including monocytes, microglia, macrophages, and dendritic cells.

ABSTRACT:

The innate immune system plays important roles in ocular pathophysiology including uveitis, diabetic retinopathy, and age-related macular degeneration. Innate immune cells, specifically mononuclear phagocytes, express overlapping cell surface markers, which makes identifying these populations a challenge. Multi-parameter flow cytometry allows for the simultaneous, quantitative analysis of multiple cell surface markers in order to differentiate monocytes, macrophages, microglia, and dendritic cells in mouse eyes. This protocol describes the enucleation of whole mouse eyes, ocular dissection, digestion into a single cell suspension, and staining of the single cell suspension for myeloid cell markers. Additionally, we explain the proper methods for determining voltages using single color controls and for delineating positive gates using fluorescence minus one controls. The major limitation of multi-parameter flow cytometry is the absence of tissue architecture. This limitation can be overcome by multi-parameter flow cytometry of individual ocular compartments or complimentary immunofluorescence staining. However, immunofluorescence is limited by its lack of quantitative analysis and reduced number of fluorophores on most microscopes. We describe the use of multi-parametric flow cytometry

to provide highly quantitative analysis of mononuclear phagocytes in laser-induced choroidal neovascularization. Additionally, multi-parameter flow cytometry can be used for the identification of macrophage subsets, fate mapping, and cell sorting for transcriptomic or proteomic studies.

INTRODUCTION:

The innate immune system includes multiple cell types that stimulate complement activation and inflammation. Innate immune cells include natural killer (NK) cells, mast cells, basophils, eosinophils, neutrophils, and mononuclear phagocytes. Mononuclear phagocytes, which are composed of monocytes, macrophages, and dendritic cells, have been implicated in the pathophysiology of multiple ophthalmic conditions including uveitis, diabetic retinopathy, and age-related macular degeneration (AMD)[1]. In this protocol, we will focus on the identification of mononuclear phagocytes using multi-parameter flow cytometric analysis in a mouse model of neovascular AMD[2]. This protocol is adaptable for mouse models of diabetic retinopathy and/or uveitis, but more extensive ocular dissection is recommended because of the systemic nature of these diseases.

Mononuclear phagocytes express overlapping cell surface markers. Long-lasting tissue resident macrophages and microglia originate from the yolk sac-derived erythromyeloid progenitor[3], while recycling macrophages and dendritic cells differentiate from the bone marrow-derived macrophage dendritic cell progenitor[4]. Mouse cell surface markers common to monocytes, macrophages, and dendritic cells include CD45, CD11b[5], F4/80[6], Cx3cr1[7], and the intracellular marker Iba1[8]. In order to overcome this challenge, transcriptomic analysis of macrophages, monocytes, and dendritic cells from multiple tissues defines CD64 as a macrophage-specific cell surface marker[6]. Macrophages have been described in the iris, choroid, ciliary body, and optic nerve in healthy eyes[3]. Alternatively, dendritic cell identification is more difficult; the most specific method of dendritic cell identification requires fate mapping using the Zbtb46-GFP reporter mouse[9]. Independent of this reporter line, expression of CD11c and MHCII in conjunction with the absence of CD64 can identify potential dendritic cells[6,10]. Dendritic cells have been identified in cornea, conjunctiva, iris, and choroid in normal eyes[11]. Microglia are specialized macrophages located in the retina, protected by the blood-retinal barrier, and derived from yolk sac progenitor cells[12]. As a result, retinal microglia can be differentiated from monocyte-derived macrophages by their dim levels of CD45 expression[13] and high levels of Tmem119, which is available as a flow cytometry antibody[14]. Upon microglia activation, however, CD45 can be up-regulated[15] and Tmem119 may be down-regulated[3], demonstrating the complexity of microglia biology and this is likely relevant in both AMD and its mouse model. Finally, monocytes can be divided into at least two subtypes, including classical and non-classical. Classical monocytes display $CCR2^{+}Ly6C^{high}CX3CR1^{low}$ expression, and non-classical monocytes demonstrate $CCR2^{-}Ly6C^{low}CX3CR1^{high}$ markers[5].

Due to the necessity of the quantitative analysis of marker expression, i.e., high versus low/dim levels, multi-parameter flow cytometry is the ideal method for discrimination between monocytes, macrophages, microglia, and dendritic cells in the eye and other tissues. Additional advantages include the identification of sub-populations, the ability to use fluorescence-

activated cell sorting (FACS) to sort cell populations for transcriptomic or proteomic analysis, and fate mapping. The major disadvantage of multi-parameter flow cytometry is the lack of tissue architecture. This can be overcome by the ophthalmic dissection into the various ocular subcompartments: cornea, conjunctiva, iris, lens, retina, and choroid-sclera complex. Additionally, confirmatory immunofluorescence imaging can be performed, but is limited by the number of markers and lack of robust quantitation.

Genome wide association studies have linked multiple complement genes with AMD[16]. Complement activation leads to anaphylatoxin production, leukocyte recruitment, and resultant inflammation. In complement receptor deficient mice, laser injury reduces mononuclear phagocyte recruitment and laser-induced choroidal neovascularization (CNV) area[17]. Similarly, the C-C motif chemokine receptor 2 (CCR2) knockout mouse, which is deficient in monocyte recruitment to the tissue, demonstrates both decreased mononuclear phagocyte recruitment and laser-induced CNV area[18]. These data link complement and mononuclear phagocytes with experimental CNV and possibly neovascular AMD. In support of this association, complement receptors are dysregulated on peripheral blood monocytes in patients with neovascular AMD[19,20]. These data demonstrate a strong association between AMD and mononuclear phagocytes.

In this manuscript, we will use the experimental laser induced CNV model to characterize the mononuclear phagocyte populations in the mouse eye using multi-parameter flow cytometry. Laser-induced CNV is the standard mouse model of neovascular AMD, which demonstrated the efficacy of current first line neovascular AMD therapy[21]. This protocol will describe enucleation of mouse eyes, ocular dissection, digestion into a single cell suspension, antibody staining, determination of laser voltages using single color controls, and gating strategy using fluorescence minus one (FMO) controls. For a detailed description of the laser-induced CNV model, please see a previous publication[22]. Using this protocol, we will define microglia, monocytes, dendritic cells, and macrophage populations. Furthermore, we will use MHCII and CD11c to further define macrophage subsets within the laser induced CNV model.

PROTOCOL:

All procedures were approved by the Northwestern University Institutional Animal Care and Use Committee. C57BL/6 mice were group housed at a barrier facility at the Center for Comparative Medicine at Northwestern University (Chicago, IL). All animals were housed in 12/12 h light/dark cycle with free access to food and water.

1. Collection of ocular tissue

1.1. Sacrifice 10-12-week-old C57BL/6J mice of either sex using regulated administration of carbon dioxide until mouse is unresponsive and no longer inhaling. Perform cervical dislocation or other approved secondary method to ensure euthanasia.

NOTE: Transcardial perfusion can be performed to remove circulating leukocytes that are not in the ocular tissues. In this experiment, systemic perfusion does not reduce the number of

microglia, monocytes, macrophages, or dendritic cells detected in untreated or laser treated whole eyes. Therefore, the majority of these cell types are located in the ophthalmic tissues and this step is optional.

1.2. To enucleate eyes, push down near the eye socket while placing a pair of curved forceps gently under the eye as it stands out of the socket. Pinch forceps closed under the eye without squeezing the actual eye. Dislodge eye from the surrounding conjunctiva (please see prior publication)[23].

1.3. Pull eye laterally until the optic nerve is the only remaining connection to detach the eye. The optic nerve often severs with tension, but a small scissor is sometimes necessary to cut the optic nerve. Place the eye in cold 1x Hank's Buffered Saline Solution (HBSS) with calcium and magnesium in 1.7 mL microcentrifuge tube.

2. Digestion of ocular tissue

2.1. Prepare the digestion buffer containing 0.1 mg/mL digestion enzyme and 0.2 mg/mL DNase in cold HBSS. Reconstitute 5 mg digestion enzyme in 2 mL of sterile water initially. Prepare an initial dilution of 10 mg/mL DNase in HBSS. For every 10 mL of the digestion buffer (sufficient for 3 animals) mix 9.4 mL of cold HBSS with 0.4 mL of reconstituted digestion enzyme and 0.2 mL of diluted DNase I.

NOTE: These concentrations were empirically determined over multiple experiments to provide optimal levels of antibody staining of single cells, while reducing cell death. Collagenase D was tried as an alternative to digestion enzyme with reduced cell viability and decreased $CD45^+$ cells. Please see **Discussion** for more details regarding the iterative process to optimize digestion.

2.2. Under a dissecting microscope at 10x total magnification, remove the remaining conjunctiva and optic nerve using fine forceps and spring scissors in cold HBSS.

2.3. Move clean eyes to a dry dissecting dish or small weigh boat. Inject 0.15-0.20 mL/eye of digestion buffer via syringe fitted with 30 G needle into the vitreous cavity after two perforating wounds are made in the eye through the visual axis and 90˚ away from this first wound for digestion buffer egress.

2.4. Mince whole eyes using spring scissors and fine forceps with all pieces smaller than 0.5 mm x 0.5 mm. Dissociate lens tissue with blunt mechanical disruption via forceps to prevent clogging pipette tips in subsequent steps. For each sample, rinse forceps and scissors each with 0.75 mL of digestion buffer into small dish. Use a new dish for each sample.

2.5. Transfer contents of the dish to a dissociation tube on ice using P1,000 pipette taking care to not lose any material in the pipette transfer. Rinse the dish with additional 1.5 mL of digestion buffer bringing the total volume in dissociation tube to 3.25-3.50 mL.

2.6. Place the dissociation tube inverted onto electronic dissociator and run cycle "m_brain_03_01", consisting of 1 min unidirectional rotation at 200 rpm at room temperature, which is a pre-loaded program. Ensure all tissue is at the bottom of the dissociation tube in contact with digestion buffer for this and all remaining steps.

2.7. Place the dissociation tube in shaking incubator for 30 min at 200 rpm at 37 ˚C.

2.8. Repeat steps 2.6 and 2.7 one additional time. Following second 30 min incubation perform one final mechanical digestion using electronic dissociator as in step 2.6.

2.9. Stop the reaction by adding 10 mL of cold flow buffer and place tubes on ice.

3. Preparation of cell suspension

3.1. To create single-cell suspension, pour the halted eye digestion reaction through a 40 µm filter placed on the top of a 50 mL conical centrifuge tube. Using the plunger from a 2.5 mL syringe, push any remaining pieces of undigested eye tissue through the filter.

3.2. Wash the dissociation tube with 10 mL of Flow buffer and rinse filter before using the same plunger to again pass undigested eye tissue pieces through the filter.

3.3. Repeat step 3.2 using 5 mL of Flow buffer.

3.4. Wash the dissociation tube and filter with a final 10 mL of Flow buffer.

NOTE: Total volume of digestion and flow buffer is about 38-40 mL for each sample.

3.5. Centrifuge the conical tube at 400 *x g* for 10 min at 4 ˚C. Decant the supernatant without disturbing the cell pellet.

3.6. Prepare 1x lysing solution by adding 10x lysing to sterile water. Break up the pellet by flicking tube against another tube. To lyse red blood cells, add 1 mL of 1x lysing solution for 30 s with swirling at room temperature (RT).

3.7. Stop the reaction with 20 mL of Flow buffer.

3.8. Centrifuge the conical tube at 400 *x g* for 10 min at 4 ˚C. Decant the supernatant without disturbing the cell pellet.

3.9. Dissociate the pellet by flicking tube against another tube. Add 5 mL of cold 1x HBSS per tube.

3.10. Centrifuge tubes at 400 *x g* for 10 min at 4 ˚C. Aspirate supernatant.

4. Staining of cell suspension for mononuclear phagocytes

4.1. Prepare 0.5 mL of Live/Dead stain per sample by diluting Live/Dead dye 1:5,000 in cold HBSS.

4.2. Add Live/Dead stain to each sample using a P1,000 pipette making sure to dissociate the pellet completely. Transfer samples to 1.2 mL micro titer tubes.

4.3. Take a small aliquot (10 µL) to count cells using a hemocytometer or automatic cell counter (see 4.4). Incubate samples with Live/Dead stain for 15 min at room temperature in the dark.

4.4. Count cells using Trypan blue to determine the number of live cells per sample.

NOTE: Typically, 2 eyes from a 10-12-week-old C57BL/6J mouse contain less than 2 x 10^6 living cells.

4.5. Wash samples by adding 400 µL of cold Flow buffer. Centrifuge tubes in a micro titer tube rack at 400 *x g* for 10 min at 4 ˚C. Aspirate the supernatant without disturbing the cell pellet.

4.6. Resuspend cells completely in 500 µL of cold Flow buffer. Centrifuge tubes in a micro titer tube rack at 400 *x g* for 10 min at 4 ˚C. Aspirate the supernatant without disturbing the cell pellet.

4.7. Block up to 5 x 10^6 living cells in 50 µL of F_c block (1:50 dilution in cold Flow buffer of purified rat anti-mouse CD16/CD32). If more than 5 x 10^6 living cells, increase volumes appropriately.

4.8. Add F_c block to the pellet making sure to completely dissociate the sample. Incubate for 20 min at 4 ˚C.

4.9. Add 50 µL of antibody staining solution (see **Table 1** for choice and amount of each antibody that is included in the solution) per 5 x 10^6 living cells directly to cells in F_c block and mix completely. Incubate for 30 min at 4 ˚C.

NOTE: Antibody quantities are dependent upon the flow cytometer configuration and should be titrated independently for every lab and instrument. See **Table 2** for instrument configuration of filters and mirrors. To titrate antibodies, start with manufacturer's recommendation, and calculate the staining index. Perform a test run of varying antibody concentrations (both above and below the manufacturer's recommendation) and choose the lowest concentration of antibody where the staining index is maintained. Also, ensure that positive staining that is less bright than the single-color control. Use unstained cells to ensure that negatively stained cells are on scale and have a peak at or less than 1 x 10^2. Use a fluorescence minus one control to define the positively stained cells.

4.10. Wash samples by adding 700 µL of cold Flow buffer. Centrifuge tubes in a micro titer tube rack at 400 *x g* for 10 min at 4 ˚C. Aspirate the supernatant without disturbing the cell pellet.

4.11. Optionally, after antibody staining, the samples can be fixed with 500 µL of 2% paraformaldehyde in Flow buffer. Fix samples for 15 min at room temperature. Then, perform one wash as described in 4.10. Store fixed samples at 4 ˚C. Count beads should be added on the day of flow cytometry data collection. Fixed samples should be run on flow cytometer in 1-2 days.

CAUTION: Paraformaldehyde is a corrosive and a health hazard.

4.12. Wash samples again using 500 µL of cold Flow buffer. Centrifuge tubes in a micro titer tube rack at 400 *x g* for 10 min at 4 ˚C. Aspirate half of the supernatant without disturbing the cell pellet.

4.13. Resuspend pellets and transfer to a 96 well, U-bottom assay plate. Centrifuge plate at 400 *x g* for 5 min at 4 ˚C. To decant the supernatant, turn plate over and in one strong shake dislodge the liquid into a sink basin, without disturbing pellet.

4.14. In a new 1.2 mL micro titer tube, place 50 µL of well vortexed count beads.

4.15. Resuspend pellets in 96 well plate in 200 µL of cold Flow buffer. Add cell mixture on the top of beads from prior step. Run on flow cytometer in total volume of 250 µL / micro titer tube.

5. Collection of flow cytometry data

5.1. Turn on and prepare flow cytometer. Instructions listed here are for a modified four laser cytometer (**Table 2**).

5.2. Run a test sample, which includes a small aliquot from each sample, to ensure that all cells are on scale for each detector. Adjust voltages so that all cells are on scale.

5.3. Run single color controls (SCC) for every fluorophore used in staining cocktail (**Table 3**). Place micro titer tube into a larger 5 mL polystyrene tube for placement onto the flow cytometer stage.

NOTE: Root fluorophores like BV421 (Pacific Blue), FITC, PE, Alexa647 (APC), and Alexa700 do not require the same antibody as the cocktail (i.e., CD19 PE for CD64 PE). However, tandem fluorophores like PE-CF594, PE-Cy7, or APC-Cy7 require the same antibody for SCC as cocktail due to potential dissociation of the conjugated fluorophores.

5.3.1. Create the SCC for BV421 by adding 2 drops of compensation beads to a 1.2 mL titer tube along with 1 µL of hamster anti-mouse CD11c BV421. Compensation beads are used because CD11c BV421 is an IgG lambda subtype rather than kappa as described in 5.3.3. Incubate for 15

mins at 4 ˚C. Add 0.2 mL of flow buffer.

5.3.2. Create the SCC for the Live/Dead dye by adding one drop of positive staining beads (green cap) from the amine reactive beads, followed by 1 μL of Live/Dead dye. Incubate for 15 min at room temperature in the dark. Add one drop of the negative beads (white cap) from the amine reactive beads. Add 0.2 mL of flow buffer.

5.3.3. Create the remaining SCCs by adding one drop of positive staining beads (green cap) from the anti-rat and anti-hamster Ig kappa bead set, followed by the antibody quantity listed (**Table 3**) in a 1.2 mL titer tube. Incubate for 15 min at 4 ˚C. Add one drop of the negative beads (white cap) from the anti-rat and anti-hamster Ig kappa bead set. Add 0.2 mL of flow buffer.

5.3.4. Vortex all bead mixtures completely. Store SCCs at 4 ˚C for up to 3 days.

NOTE: The SCC for fluorescent reporter mice is unstained cells.

5.3.5. When running SCCs, set voltages such that the SCC sample has a peak greater than any fluorescence for a sample of cells in the same detector channel. In addition, voltages should be set so that any SCC has at least a 0.5 Log difference between the histogram peak in the channel of interest versus any other channel (**Figure 1**).

5.4. Run samples on "Low" keeping events/second below 4000. If flow rate cannot be lowered appropriately, dilute samples with additional cold flow buffer. Record the volume added as this will be necessary for the count calculation (see representative results).

5.5. Collect at least 3 x 10^6 events per sample. This may be higher than the cell number due to pigment granules and debris counting as events on your cytometer.

5.6. Record a Fluorescence Minus One (FMO) for each fluorophore other than Live/Dead for proper gating strategy in section 6.4. An FMO is a sample that has been stained with all fluorophores except one.

5.7. Clean and shut down flow cytometer according to manufacturer or facility instructions.

6. Annotation of flow cytometry data

6.1. Open a new worksheet using analysis software. Import FCS files from cytometer for all samples and single-color controls.

6.2. Use SCCs to create a compensation matrix.

6.3. Apply the compensation matrix to your stained samples and FMOs.

6.4. Use the FMOs to determine positive staining to draw gates.

REPRESENTATIVE RESULTS:

Figure 1 showed uncompensated frequency histograms for the SCCs and cells for the red laser: Alexa647, Alexa700, and APC-Cy7. In **Figure 1A**, the magenta line depicted the peak of the SCC for Alexa647, while the cyan line depicts the intended 0.5 Log difference. Notice that the peak in Alexa700 and APC-Cy7 was to the left (less bright) of the cyan line. Also note that the cells were all to the left of the magenta line. Any cells to the right of the SCC peak were not compensated. Specific channels were known to spill into others based on the chemistry of the fluorochrome dyes (i.e. Violet Laser: BV421 -> V500, Yellow-Green Laser: PE -> PE-CF594, Red Laser: Alexa647 -> Alexa700, Alexa700 -> APC-Cy7, Cross Laser: PE-Cy7 -> APC-Cy7). If either of the above conditions were not met, the voltage of one channel could be adjusted upward while any spill channels could be moved down. See **Figure 1B** and **Figure 1C** for additional examples of the red laser. Once the voltages were determined and then recorded, all samples must be run with the voltage parameters. A compensation set up wizard exists and may be helpful.

Count bead identification is necessary for quantification of cell counts. **Figure 2A** showed FSC-A vs SSC-A properties for all analyzed events from two eyes of a single mouse. It is important to adjust the SSC voltage to make sure your count beads are visible as a very tight collection of SSC-A^{high} and FSC-A^{low} events. Bead counts were cleaned and confirmed by plotting PE vs APC-Cy7 (Fig 2B). Clean beads were a tight cluster of PE^{+} and APC-$Cy7^{-}$ events.

Singlets and live cells were next identified from all events. Singlets were determined by plotting FSC-H vs FSC-A. Singlets were positively correlated in these two properties while doublet and triplet cells had greater FSC-A than FSC-H (**Figure 2C**). Live cells were delineated by plotting Live / Dead vs FSC-A. Dead cells were Live / Dead positive, and cells demonstrate greater FSC-A than debris (Fig 2D). Note that count beads were Live / $Dead^{+}$ and were removed at this step.

Figure 3 shows the initial gating strategy for the delineation of mononuclear phagocytes from live, singlet cells. Live singlets were visualized using a CD45 versus CD11b plot (**Figure 3**, left). Note that $CD45^{+}CD11b^{-}$ (mostly B-cells and T-cells), $CD45^{dim}CD11b^{+}$ (putative microglia), and $CD45^{+}CD11b^{+}$ cells (infiltrating immune cells, increased with laser [Fig 3B, left]) were selected. The absence of $CD45^{+}$ cells in the CD45 FMO confirmed the gate selection (**Figure 3C**, left). Next, neutrophils, eosinophils, B-cells, NK cells, and T-cells were excluded by plotting $CD45^{+}$ live singlets using Lineage gate (Lin: Ly6G [neutrophils], SiglecF [eosinophils], B220 [B-cells], NK1.1 [NK cells], CD4 [T-cells], and CD8 [T-cells]) vs CD11b. The increase in $CD11b^{+}Lin^{-}$ cells between No Laser (**Figure 3A**, middle) and Laser (**Figure 3B**, middle) groups was easily observed. Note the lack of $CD11b^{+}$Lin- cells in the CD11b FMO (**Figure 3C**, middle) and the lack of Lin^{+} cells in the Lin FMO (**Figure 3C**, right). Microglia can be separated from infiltrating mononuclear phagocytes by the quantity of CD45 expression[13,24]. $CD11b^{+}Lin^{-}$ cells were visualized using a CD11b vs CD45 plot to identify $CD45^{dim}$ putative microglia and $CD45^{high}$ infiltrating mononuclear phagocytes. The relative increase in $CD45^{high}$ mononuclear phagocytes was clear in the Laser-treated mouse (**Figure 3A,B**, right).

Figure 4 identified microglia, three macrophage subsets, monocytes, and dendritic cells. Microglia were determined by plotting $CD45^{dim}$ cells on a CD64 vs MHCII plot (**Figure 4**, left panel). Microglia have been shown to be $CD64^{+}MHCII^{low}$ previously[13]. Microglia were relatively unchanged with laser and absent in the CD64 FMO (**Figure 4A,C** left). $CD45^{high}$ cells were next plotted on the same CD64 vs MHCII graph. $CD64^{+}MHCII^{-}$ macrophages ($MHCII^{-}$ Macs), $CD64^{-}MHCII^{-}$ monocytes, and $MHCII^{+}$ cells were identified (**Figure 4A,B**, middle left). Note the absence of $MHCII^{+}$ cells in the MHCII FMO (**Figure 4C**, middle left). $MHCII^{+}$ cells were further discriminated using CD64 and CD11c. $CD64^{+}CD11c^{-}$ macrophages ($CD11c^{-}$ Macs), $CD64^{+}CD11c^{+}$ macrophages ($CD11c^{+}$ Macs), and $CD64^{-}CD11c^{+}$ dendritic cells (DCs) were defined (**Figure 4A,B**, middle right). Note the absence of $CD11c^{+}$ cells in the CD11c FMO (**Figure 4C**, middle right). Monocytes were subtyped as classical $Ly6C^{+}$ or non-classical $Ly6C^{-}$ monocytes (**Figure 4**, right). Note the absence of $Ly6C^{+}$ monocytes in the Ly6C FMO (**Figure 4C**, right).

Number of cells per mouse (or per 2 eyes) was calculated with the following equation:

$$Cell\ number = \frac{Sample\ volume * (Cell\ count * Bead\ volume * Concentration\ of\ beads)}{(Bead\ count * Volume\ of\ cells)}$$

Using the volumes in this method, the equation is:

$$Cell\ number\ = \frac{250\ \mu L * (Cell\ count * 50\ \mu L * Concentration\ of\ beads\ [per\ \mu L])}{(Bead\ count * 200\ \mu L)}$$

Cell count and bead count will be specific to each sample. The concentration of beads is specific to each lot of count beads and provided by the manufacturer on each vial.

Macrophages infiltrate the choroid after laser injury[25], and macrophage depletion reduces CNV area[18]. These older studies rely upon immunofluorescence imaging, which cannot reliably differentiate mononuclear phagocytes, or fewer flow cytometric markers for macrophage identification. Macrophage heterogeneity is an emerging concept in innate immunology, where macrophages are capable of performing multiple functions depending upon their origin and tissue microenvironment[12,26]. We performed multi-parameter flow cytometry on untreated and laser treated mouse eyes on Day 3 after laser injury to identify mononuclear phagocytes and macrophage heterogeneity. Laser treatment increased $MHCII^{-}$, $CD11c^{-}$, and $CD11c^{+}$ macrophages by 7.0-25.6, 2.8-7.2, and 3.9-8.2 fold respectively (**Figure 5A,C**). Dendritic cell counts were also up-regulated 4.5-4.7-fold by laser (**Figure 5F**). Microglia and monocyte counts were not affected by laser treatment (**Figure 5D,E**). No significant differences were detected with or without systemic perfusion prior to enucleation. These results demonstrate increased macrophage populations and dendritic cells after laser injury with no change to microglia or monocytes. Furthermore, these data highlight how multi-parameter flow cytometry can detect macrophage heterogeneity.

FIGURE AND TABLE LEGENDS:

Table 1: Antibody fluorophore and clones (see step 4.9). Generally, one sample is either one or two digested eyes. Add flow buffer to a tube first then each antibody. Dilutions can be made to avoid pipetting too small a volume, while changing total flow buffer volume appropriately. See Table of Materials for product number and company.

Table 2: Configuration of flow cytometer. Filter and mirror setup for a four-laser cytometer and the available fluorophores which can be detected in each channel. PMT = photomultiplier tube, FSC = forward scatter, SSC = side scatter.

Table 3: Antibody fluorophore and clones for single color controls. Each antibody should be added to the appropriate compensation bead as outlined in steps 5.3.1 – 5.3.3.

Figure 1: Representative voltage set up for the red laser. (**A**) Single color controls (SCCs) for Alexa647. On the left, the SCC for Alexa647 is shown. Left middle displays the spill of the Alexa647 SCC into the Alexa700 channel. The peak of the Alexa647 SCC is shown in magenta and the 0.5 Log goal differential is displayed in cyan. Note that the peak is to the left (less bright) than the cyan line. Middle right demonstrates the spill of the Alexa647 SCC into the APC-Cy7 channel. Right illustrates the cells in the Alexa647 channel. Note that all cells are less bright than the SCC (magenta line). (**B**) SCC for Alexa700. Middle left shows the SCC for Alexa700. Left displays the spill of the Alexa700 SCC into the Alexa647 channel. Middle right demonstrates the spill of the Alexa700 SCC into the APC-Cy7 channel. The peak of the Alexa700 SCC is shown in magenta and the 0.5 Log goal differential is displayed in cyan. Note that the peak is to the left (less bright) than the cyan line. Right illustrates the cells in the Alexa700 channel. Note that all cells are less bright than the SCC (magenta line). (**C**) SCC for APC-Cy7. Left and middle left show the spill of the APC-Cy7 SCC into Alexa647 and Alexa700, respectively. Note that both peaks are to the left of the cyan line. Middle right demonstrates the ACP-Cy7 SCC. Right illustrates the cells in the APC-Cy7 channel. Note that all cells are less bright than the SCC (magenta line).

Figure 2: Representative identification of count beads, singlets, and live cells. (**A**) Side scatter area (SSC-A) vs forward scatter area (FSC-A) for all cells on a contour plot. Count beads are identified by high SSC-A, low FSC-A, and very tight clustering of the uniform beads. (**B**) PE vs APC-Cy7 plot for clean bead gate. The arrow between A and B indicates plotting of only the count bead positive events. Clean count beads are delineated by high PE and low APC-Cy7 fluorescence. (**C**) FSC-Height (FSC-H) vs FSC-Area (FSC-A) plot of all cells demonstrates singlet cells in a positively correlated wide line. Doublets and other multiplets show greater FSC-Area than FSC-Height. (**D**) Live / Dead vs FSC-A for singlet cells. Live cells are defined as Live / Dead low and FSC-A positive. Percentages indicate percent of parent.

Figure 3: Representative identification of mononuclear phagocytes. Left: CD45 vs CD11b pseudocolor plot of live cells from unlasered (**A**), lasered (**B**), and fluorescence minus one (FMO) control. $CD45^+$ cells are defined in A-B and absent in the FMO. Note the increase of $CD45^+CD11b^+$ cells in the lasered (**B**) group. **Middle:** Pseudocolor plot of lineage (Lin) marker vs CD11b for $CD45^+$ cells. $CD11b^+Lin^-$ cells are delineated in A-B and are absent in the FMO for CD11b (bottom). **Right:**

CD11b vs CD45 plot of $CD11b^{+}Lin^{-}$ cells. $CD45^{dim}$ and $CD45^{high}$ cells are identified. Note the increase in $CD45^{high}$ cells in the lasered (B) group. Percentages indicate percent of parent.

Figure 4: Representative identification of microglia, dendritic cells, monocytes, and macrophage subsets. Left: CD64 vs MHCII pseudocolor plot of $CD45^{dim}$ cells defines microglia as $CD64^{+}MHCII^{low}$. Note the similar amount of microglia in unlasered (**A**) and lasered (**B**) groups, and the absence of microglia in the FMO control (**C**). **Middle left:** CD64 vs MHCII pseudocolor plot of $CD45^{high}$ cells defines $MHCII^{-}$ macrophages as $CD64^{+}MHCII^{-}$, monocytes as $CD64^{-}MHCII^{-}$, and $MHCII^{+}$ cells. Note the increase in MHCII- macrophages in the lasered group (B), the absence of MHCII+ cells in the FMO (C, middle), and the CD64 FMO (C, left) helped determine the cutoff for $CD64^{+}$ and $CD64^{-}$ cells. **Middle right:** CD64 vs CD11c pseudocolor plot of $MHCII^{+}$ cells. $CD11c^{-}$ macrophages were defined as $CD64^{+}CD11c^{-}$, $CD11c^{+}$ macrophages were identified as $CD64^{+}CD11c^{+}$, and dendritic cells (DCs) were delineated as $CD64^{-}CD11c^{+}$. Both macrophage subsets and dendritic cells were increased with laser (B). Note the absence of $CD11c^{+}$ cells in the FMO (C). Right: Ly6C vs Tim4 pseudocolor plot of monocytes. Classical $Ly6C^{+}$ and non-classical $Ly6C^{-}$ monocytes were identified. Note that classical $Ly6C^{+}$ monocytes were absent in the Ly6C FMO (C). Percentages indicate percent of parent.

Figure 5: Representative data for mononuclear phagocytes between unlasered and lasered mice both with and without systemic perfusion. $MHCII^{-}$ (**A**), $CD11c^{-}$ (**B**), and $CD11c^{+}$ (**C**) macrophage counts were all increased with laser. No changes were detected between unlasered and lasered microglia (**D**) or monocytes (**E**). Dendritic cells (DC) were also increased with laser (**F**). Brown Forcythe and Welch ANOVA with Dunnett's T3 multiple comparison test was used to define statistical differences due to unequal variances between groups.

DISCUSSION:

Multi-parameter flow cytometry allows for the quantitative analysis of multiple cell types in a complex tissue. In this report, we describe the flow cytometric detection of mononuclear phagocyte populations, including monocytes, dendritic cells, and macrophage subsets, after laser injury in the mouse eye. Liyanage et al recently reported a similar gating strategy to detect neutrophils, eosinophils, lymphocytes, DCs, macrophages, infiltrating macrophages, and monocytes[27]. Our gating strategy primarily differs by the addition of CD64. Liyanage et al identifies DC as $CD4^{-}CD8^{-}B220^{-}CD11b^{+}CD11c^{+}$ cells, and macrophages as $CD4^{-}CD8^{-}B220^{-}CD11b^{+}CD11c^{-}NK1.1^{-}Ly6G^{-}$ cells. We identify DC as $CD4^{-}CD8^{-}B220^{-}Ly6G^{-}SiglecF^{-}NK1.1^{-}CD11b^{+}CD11c^{+}CD64^{-}$ cells and macrophages as $CD4^{-}CD8^{-}B220^{-}Ly6G^{-}SiglecF^{-}NK1.1^{-}CD11b^{+}CD64^{+}$ cells. The use of CD64 to discriminate DC from macrophages is well established[6], and this strategy allows us to identify macrophage heterogeneity, including CD11c+ macrophages. The major limitation of this method is that it does not provide data on tissue architecture or the location of specific cells within the eye. In order to determine whether these cells are in the retina, choroid, iris, or another ocular structure, our protocol can be combined with histological methods or modified to include more extensive ophthalmic dissection to individually run multi-parameter flow cytometry on each ocular subcompartment.

We have optimized the protocol for digestion of whole mouse eyes to prevent any variance created by dissection. For example, dissection of posterior eye cups with removal of cornea, iris, and lens could create variability from retained iris or corneal material (under-dissection) or increased laser injury to normal posterior eye cup area (over-dissection). Our comparison between control unlasered and lasered eyes detects the infiltration of mononuclear phagocytes because of retinochoridal injury. For the analysis of the effects of systemic diseases upon the eye, i.e. uveitis and diabetes, individual ocular subcompartment analysis is essential. The method of digestion, in section 2 of the protocol, is the most critical, while other steps in sections 3 - 5 have been used successfully on multiple tissue types[24]. We arrived at our digestion conditions through an iterative method that involved: (1) testing of chemical digestion method (Collagenase D vs digestion enzyme), (2) determination of length of chemical digestion (30, 60, and 90 minutes), and (3) addition of mechanical digestion (none, once, twice, three times). At each step we judged the success of the digestion conditions by cell viability and number of $CD45^{Hi}CD64^{+}$ (infiltrating macrophages) cells. We found that digestion enzyme (see Supplementary Table of Materials) recovered more live cells than Collagenase D and attempting half of the digestion enzyme concentration resulted in fewer infiltrating macrophages. Next, 60 minutes of chemical digestion with mechanical digestion nearly doubled the infiltrating macrophage populations. Three mechanical digestions were optimal with 25-30% live cells of singlets and the most infiltrating macrophage populations. Finally, faster mechanical digestion conditions caused severe loss of both live cells and macrophages.

In the future, we propose extending the method by removing the cornea, iris, and lens followed by separately digesting the retina and the posterior eye cup (sclera, choroid and retinal pigmented epithelium). With this modification, we expect to reduce the digestion conditions because of the proteinaceous and dense characteristics of the lens and cornea respectively. These reductions could include reduced digestion enzyme concentration, switching to Collagenase, decreased time of digestion, or diminished amount of mechanical digestion. We expect overall reduced digestion conditions for the posterior eye cup, and further diminished digestion conditions for retina alone.

Additional future directions include the expansion of our conventional multi-parameter flow cytometry panel to a conventional 6 laser instrument or spectral flow cytometry. Spectral flow cytometry allows for fluorophore detection across the entire spectrum, rather than determined by the available filters. Spectral flow cytometry results in more specific color detection. However, spectral flow cytometry requires an entirely new set of considerations to be followed and is beyond the scope of this manuscript. For more details, please see this recent JoVE article[28]. The 6 laser instruments include an ultraviolet laser, which adds 6-9 detectors. When adding markers to a mouse eye flow cytometry panel, we recommend detection of more ocular cell types. For example, the Lineage gate could be separated to detect neutrophils, eosinophils, mast cells, NK cells, and lymphocytes independently. It is not recommended to increase the subset detection of mononuclear phagocytes because of the small number of macrophages at steady state. When adding new antibodies, we suggest careful antibody titration.

In summary, we have presented an adaptable, robust method for the detection of mononuclear

phagocyte populations in the mouse eye. Due to the highly overlapping cell surface markers of monocytes, dendritic cells, macrophages, and microglia, multi-parameter flow cytometry is the best method to detect these cellular populations. Flow cytometry can be used for analysis of cell types, fate mapping, and/or cell sorting for transcriptomic or proteomic evaluation. Its major limitation is lack of tissue architecture, and key findings can be confirmed using traditional histology.

ACKNOWLEDGMENTS:

JAL was supported by NIH grant K08EY030923; CMC was supported by a K01 grant (5K01AR060169) from the NIH National Institute of Arthritis and Musculoskeletal Diseases and a Novel Research Grant (637405) from the Lupus Research Alliance.

DISCLOSURES:

The authors have nothing to disclose.

REFERENCES:

1. Chinnery, H. R., McMenamin, P. G., Dando, S. J. Macrophage physiology in the eye. *Pflugers Archiv: European Journal of Physiology.* **469** (3-4), 501–515 (2017).
2. Droho, S., Cuda, C. M., Perlman, H., Lavine, J. A. Monocyte-Derived Macrophages Are Necessary for Beta-Adrenergic Receptor-Driven Choroidal Neovascularization Inhibition. *Investigative Ophthalmology & Visual Science.* **60** (15), 5059–5069 (2019).
3. O'Koren, E. G. et al. Microglial Function Is Distinct in Different Anatomical Locations during Retinal Homeostasis and Degeneration. *Immunity*. **50** (7), 723–727 (2019).
4. Kratofil, R. M., Kubes, P., Deniset, J. F. Monocyte Conversion During Inflammation and Injury. *Arteriosclerosis, Thrombosis, and Vascular Biology.* **37** (1), 35–42 (2017).
5. Zimmermann, H. W., Trautwein, C., Tacke, F. Functional role of monocytes and macrophages for the inflammatory response in acute liver injury. *Frontiers in Physiology.* **3**, 56 (2012).
6. Gautier, E. L. et al. Gene-expression profiles and transcriptional regulatory pathways that underlie the identity and diversity of mouse tissue macrophages. *Nature Immunology.* **13** (11), 1118–1128 (2012).
7. Sutti, S. et al. CX3CR1 Mediates the Development of Monocyte-Derived Dendritic Cells during Hepatic Inflammation. *Cells.* **8** (9), 1099–1015 (2019).
8. Liu, J. et al. Myeloid Cells Expressing VEGF and Arginase-1 Following Uptake of Damaged Retinal Pigment Epithelium Suggests Potential Mechanism That Drives the Onset of Choroidal Angiogenesis in Mice. *PLoS One.* **8** (8), e72935 (2013).
9. Satpathy, A. T. et al. Zbtb46 expression distinguishes classical dendritic cells and their committed progenitors from other immune lineages. *The Journal of Experimental Medicine.* **209** (6), 1135–1152 (2012).
10. Krause, T. A., Alex, A. F., Engel, D. R., Kurts, C., Eter, N. VEGF-Production by CCR2-Dependent Macrophages Contributes to Laser-Induced Choroidal Neovascularization. *PLoS One.* **9** (4), e94313 (2014).
11. Lin, W., Liu, T., Wang, B., Bi, H. The role of ocular dendritic cells in uveitis. *Immunology*

Letters. **209**, 4–10 (2019).
12. Ginhoux, F., Schultze, J. L., Murray, P. J., Ochando, J., Biswas, S. K. New insights into the multidimensional concept of macrophage ontogeny, activation and function. *Nature Immunology.* **17** (1), 34–40 (2016).
13. O'Koren, E. G., Mathew, R., Saban, D. R. Fate mapping reveals that microglia and recruited monocyte-derived macrophages are definitively distinguishable by phenotype in the retina. *Science Reports.* **6**, 20636 (2016).
14. Bennett, M. L. et al. New tools for studying microglia in the mouse and human CNS. *Proceedings of the National Academy of Sciences U.S.A.* **113** (12), E1738–E1746 (2016).
15. Müller, A., Brandenburg, S., Turkowski, K., Müller, S., Vajkoczy, P. Resident microglia, and not peripheral macrophages, are the main source of brain tumor mononuclear cells. *International Journal of Cancer.* **137** (2), 278–288 (2014).
16. McHarg, S., Clark, S. J., Day, A. J., Bishop, P. N. Age-related macular degeneration and the role of the complement system. *Molecular Immunology.* **67** (1), 43–50 (2015).
17. Nozaki, M. et al. Drusen complement components C3a and C5a promote choroidal neovascularization. *Proceedings of the National Academy of Sciences U.S.A.* **103** (7), 2328–2333 (2006).
18. Tsutsumi, C. The critical role of ocular-infiltrating macrophages in the development of choroidal neovascularization. *Journal of Leukocyte Biology.* **74** (1), 25–32 (2003).
19. Subhi, Y. et al. Association of CD11b +Monocytes and Anti–Vascular Endothelial Growth Factor Injections in Treatment of Neovascular Age-Related Macular Degeneration and Polypoidal Choroidal Vasculopathy. *JAMA Ophthalmology.* **137** (5), 515–518 (2019).
20. Singh, A. et al. Altered Expression of CD46 and CD59 on Leukocytes in Neovascular Age-Related Macular Degeneration. *AJOPHT.* **154** (1), 193–199 (2012).
21. Kwak, N., Okamoto, N., Wood, J. M., Campochiaro, P. A. VEGF is major stimulator in model of choroidal neovascularization. *Investigative Ophthalmology & Visual Science.* **41** (10), 3158–3164 (2000).
22. Shah, R. S., Soetikno, B. T., Lajko, M., Fawzi, A. A. A Mouse Model for Laser-induced Choroidal Neovascularization. *Journal of Visualized Experiments.* (106), e53502 (2015).
23. Mahajan, V. B., Skeie, J. M., Assefnia, A. H., Mahajan, M., Tsang, S. H. Mouse Eye Enucleation for Remote High-throughput Phenotyping. *Journal of Visualized Experiments* (57), e3814 (2011).
24. Makinde, H. M. et al. A Novel Microglia-Specific Transcriptional Signature Correlates with Behavioral Deficits in Neuropsychiatric Lupus. *Frontiers in Immunology.* **11**, 338–419 (2020).
25. Sakurai, E., Anand, A., Ambati, B. K., van Rooijen, N., Ambati, J. Macrophage depletion inhibits experimental choroidal neovascularization. *Investigative Ophthalmology & Visual Science.* **44** (8), 3578–3585 (2003).
26. Murray, P. J. et al. Macrophage activation and polarization: nomenclature and experimental guidelines. *Immunity.* **41** (1), 14–20 (2014).
27. Liyanage, S. E. et al. Flow cytometric analysis of inflammatory and resident myeloid populations in mouse ocular inflammatory models. *Experimental Eye Research.* **151**, 160–170 (2016).
28. Schmutz, S., Valente, M., Cumano, A., Novault, S. Analysis of Cell Suspensions Isolated from Solid Tissues by Spectral Flow Cytometry. *Journal of Visualized Experiments.* (123), e55578

656 (2017).

Fig 1

Click here to access/download;Figure;Jove Fig 1 v1.psd

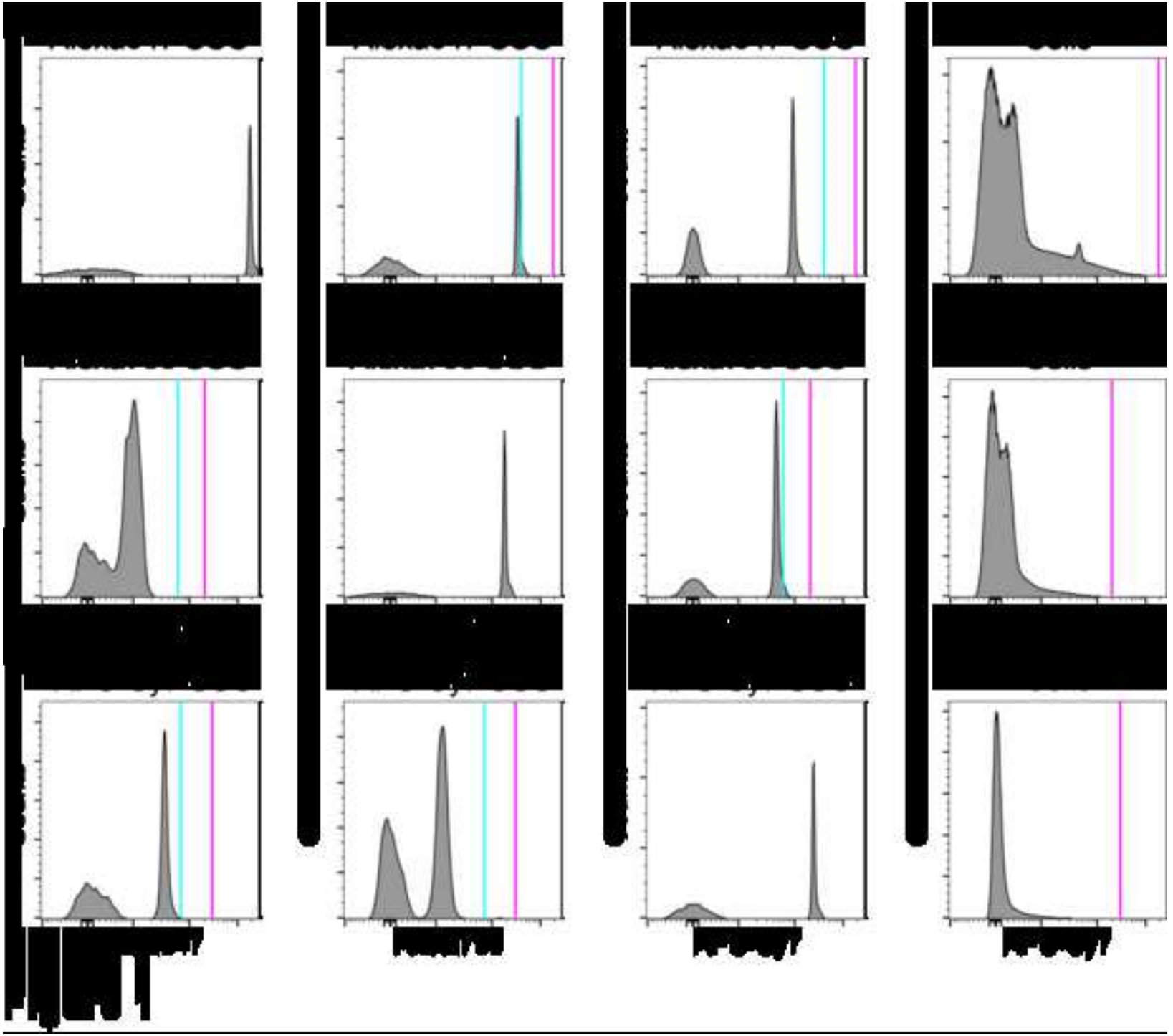

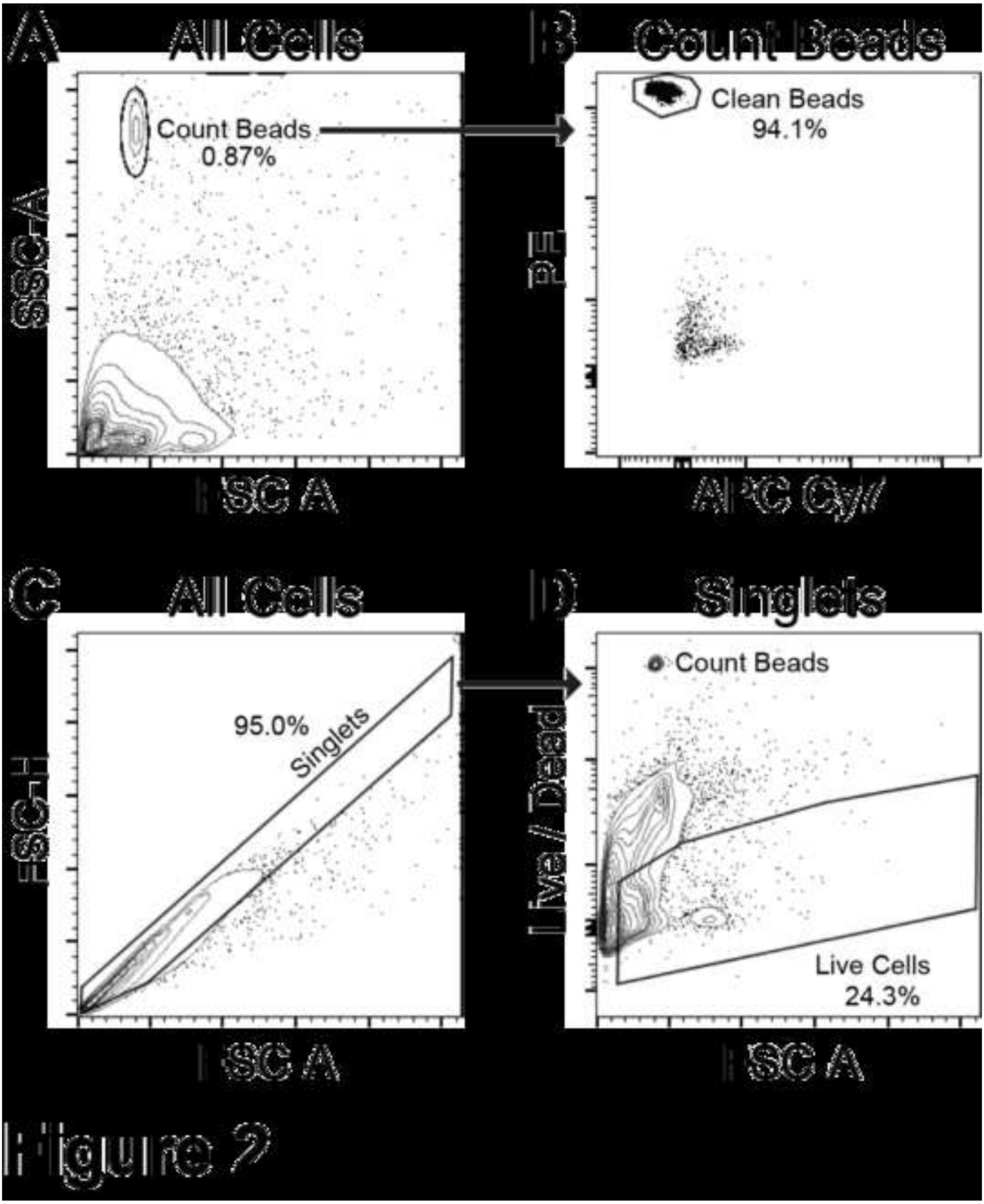

Figure 2

Fig 3

Click here to access/download;Figure;Jove Fig 3 v2.psd

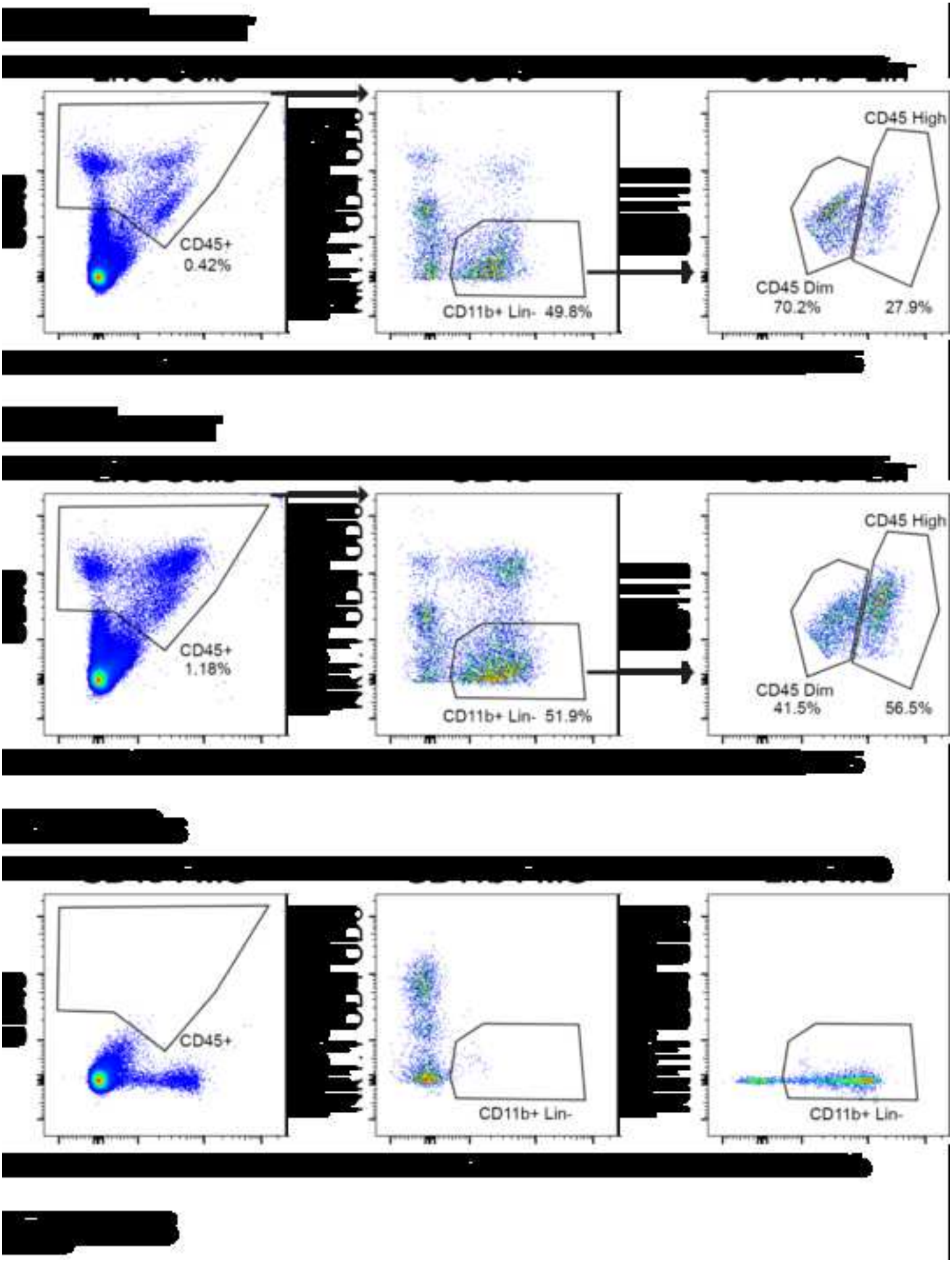

Fig 4

Click here to access/download;Figure;Jove Fig 4 v3.psd

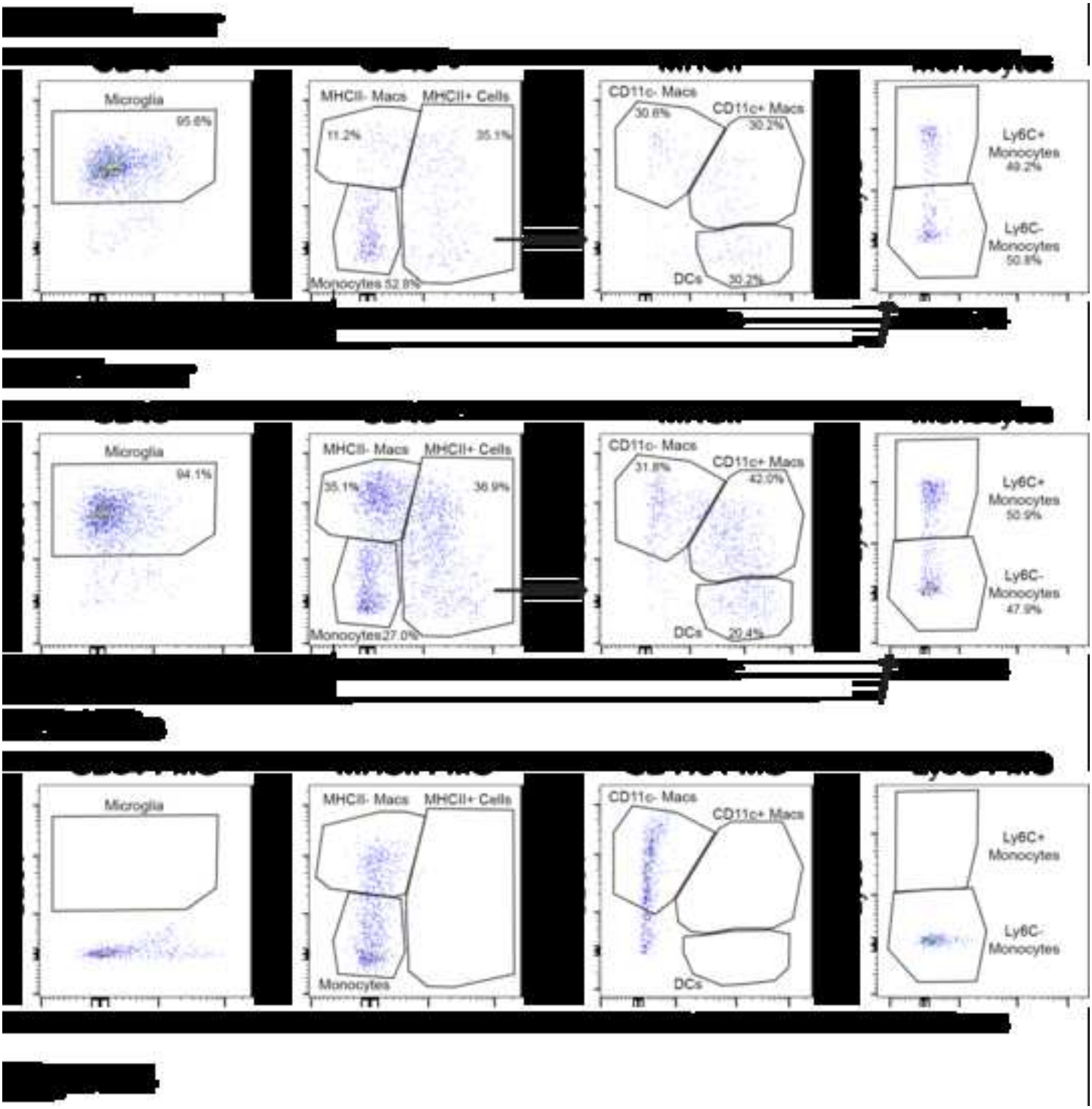

Fig 5

Click here to access/download;Figure;JOVE Fig 5 v2.psd

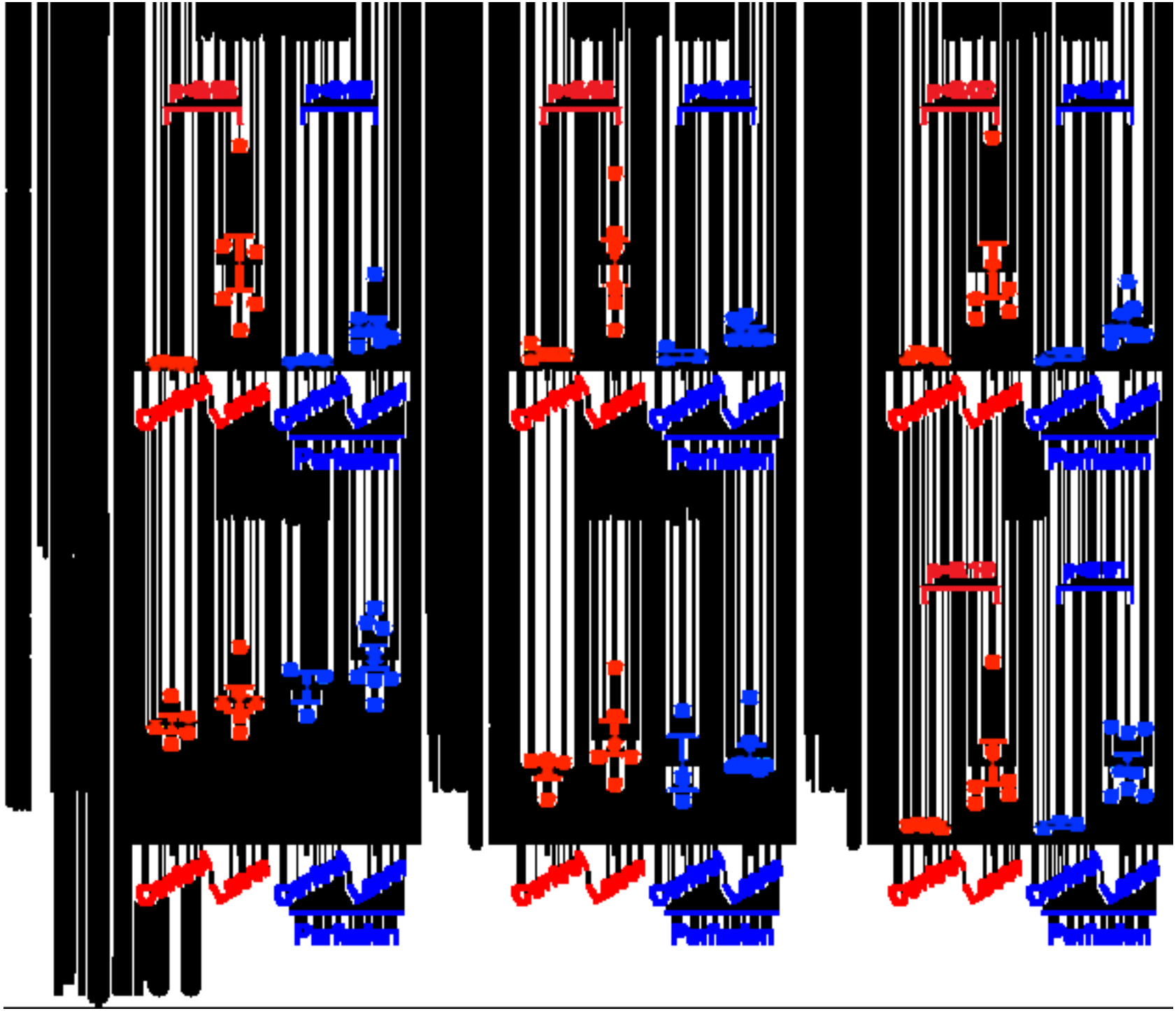

Table 1

Antibody or buffer	Fluorophore	Clone
rat anti-mouse Ly6C	FITC	AL-21
mouse anti-mouse CD64	PE	X54-5/7.1
rat anti-mouse Tim4	AlexaFluor 647	RMT4-54
hamster anti-mouse CD11c	BV 421	HL3
rat anti-mouse Ly6G	PE-CF594	1A8
mouse anti-mouse NK1.1	PE-CF594	PK136
rat anti-mouse Siglec F	PE-CF594	E50-2440
rat anti-mouse B220	PE-CF594	RA3-6B2
rat anti-mouse CD8	PE-CF594	53-6.7
rat anti-mouse CD4	PE-CF594	RM4-5
rat anti-mouse MHC II	AlexaFluor 700	M5/114.15.2
rat anti-mouse CD11b	APC-Cy7	M1/70
rat anti-mouse CD45	PE-Cy7	30-F11
MACS buffer		

Amount per sample (ng)
15
40
300
300
10
10
20
20
40
20
2.5
2
6

Table 2

Laser	PMT Slot	Filter
Violet (405nm)	A	525/50
	B	450/50
Blue (488nm/FSC)	A	710/50
	B	525/50
	C	488/10
Yellow-Green (561nm)	A	780/60
	B	610/20
	C	582/15
Red (640nm)	A	780/60
	B	730/45
	C	670/30

Mirror	Colors
505LP	V500 or AmCyan
	Pacific Blue, eFluor 450, V450 or BV421
685LP	PerCP-Cy5.5, PerCP, PI or 7AAD
505LP	FITC, CFSE, GFP or AlexaFluor 488
	SSC
735LP	PE-Cy7
600LP	PE-CF594, mCherry or DsRed2
	PE
735LP	APC-Cy7, APC-H7 or APC-eFluor 780
690LP	AlexaFluor 700
	APC or AlexaFluor 647

Table 3

Antibody	Fluorophore	Clone
rat anti-mouse CD45	FITC	30-F11
rat anti-mouse CD19	PE	1D3
rat anti-mouse Tim4	AlexaFluor 647	RMT4-54
hamster anti-mouse CD11c	BV421	HL3
rat anti-mouse Siglec F	PE-CF594	E50-2440
rat anti-mouse CD19	AlexaFluor 700	1D3
rat anti-mouse CD11b	APC-Cy7	M1/70
rat anti-mouse CD45	PE-Cy7	30-F11
Live / Dead Dye	eFluor 506	N/A

Amount per SCC (ng)
500
40
100
200
40
200
200
200
1 μl

Name of Material/ Equipment	Company	Catalog Number	Comments/Description
0.6 ml microcentrifuge tubes	Fisher Scientific	05-408-120	
1.7 ml microcentrifuge tubes	Costar	3620	
10 ml pipettes	Fisher Scientific	431031	
15 ml conicals	ThermoFisher	339650	
1x HBSS, 500 ml	Gibco	14025-092	
2.5 ml syringe	Henke Sass Wolf	7886-1	
20% paraformaldehyde solution	Electron Microscopy Sciences	15713-S	
25 ml pipettes	Fisher Scientific	431032	
30 G needle	Exel	26437	
3ml luer lock syringe	Fisher Scientific	14955457	
41 x 41 x 8 mm polystyrene weigh dish	Fisher Scientific	08-732-112	
50 ml conicals	Falcon	352070	
96-well, U-bottom assay plate without lid	Falcon	353910	
Amine reactive beads	ThermoFisher	A10628	
Analysis software	FlowJo	v 10	
Anti-rat and anti-hamster Ig kappa bead set	BD Biosciences	552845	
C57BL/6J mice	Jackson Laboratory	664	
Cell counter	Invitrogen	AMQAX1000	
Cell counter slides	Invitrogen	C10283	
Compensation beads	ThermoFisher	01-1111-42	
Count beads	ThermoFisher	01-1234-42	
Curved forceps	Fisher Scientific	16-100-123	
Digestion enzyme	Sigma Aldrich	5401020001	
Dissecting microscope	National Optical and Scientific Instruments, Inc.	DC3-420T	
Dissociation tubes	Miltenyi Biotec	130-096-334	
DNase	Roche	10104159001	
Electronic dissociator	Miltenyi Biotec	130-095-937	
FACS Diva software	BD Biosciences		

Fc block, rat anti-mouse CD16/CD32	BD Biosciences	553142
Fine forceps	Integra Miltex	17035X
Flow buffer	Miltenyi Biotec	130-091-221
Flow cytometer	BD Biosciences	
Flow tubes	Falcon	352008
Hamster anti-mouse CD11c BV421	BD Biosciences	562782
Ice bucket	Fisher Scientific	07-210-123
Live/Dead dye	ThermoFisher	65-0866-14
Lysing solution, 10x solution	BD Biosciences	555899
Micro titer tube and rack	Fisher Scientific	02-681-380
Mouse anti-mouse CD64 PE	BioLegend	139304
Mouse anti-mouse NK1.1 PECF594	BD Biosciences	562864
P1000 pipet tips	Denville Scientific	P2404
P1000 pipettor	Gilson	FA10006M
P2 pipet tips	eppendorf	22491806
P2 pipettor	Gilson	FA10001M
P20 pipettor	Gilson	FA10003M
P200 pipet tips	Denville Scientific	P2401
P200 pipettor	Gilson	FA10005M
Pipet man	Fisher Scientific	FB14955202
Rat anti-mouse B220 PECF594	BD Biosciences	562313
Rat anti-mouse CD11b APC-Cy7	BD Biosciences	557657
Rat anti-mouse CD19 AlexaFluor 700	BD Biosciences	557958
Rat anti-mouse CD19 PE	BD Biosciences	553786
Rat anti-mouse CD4 PECF594	BD Biosciences	562314
Rat anti-mouse CD45 FITC	ThermoFisher	11-0451-82
Rat anti-mouse CD45 PE-Cy7	BD Biosciences	552848
Rat anti-mouse CD8 PECF594	BD Biosciences	562315
Rat anti-mouse Ly6C	BD Biosciences	561085
Rat anti-mouse Ly6G PECF594	BD Biosciences	562700
Rat anti-mouse MHC II AlexaFluor 700	BioLegend	107622
Rat anti-mouse Siglec F PECF594	BD Biosciences	562757
Rat anti-mouse Tim4 AlexaFluor647	BD Biosciences	564178

Shaking incubator	Labnet	311DS
Spring scissors	Fine Science Tools	15024-10
Sterile cell strainer, 40 μm nylon mesh	Fisher Scientific	22363547
Sterile water, 500 ml	Gibco	A12873-01
Swinging bucket centrifuge	eppendorf	5910 R
Trypan blue, 0.4% solution	Gibco	15250061

Editorial Comments:

1. Title Comment Regarding “Multi-Parameter Flow Cytometric Analysis”: This part is not highlighted in the text. Please make the title reflect the highlighted section as this will be shown in the video. Or change the highlight accordingly.

Response: We have amended the title to say Digestion of Whole Mouse Eyes for Multi-Parameter Flow Cytometric Analysis of Mononuclear Phagocytes. The entire goal of this protocol is to perform multi-parameter flow cytometry. The highlighted section of the text includes the digestion of mouse eyes, preparation of the digestion into a single cell suspension, followed by the staining of the cell suspension with a cocktail of cell surface markers in order to perform multi-parameter flow cytometry. The highlighted section does not include the actual running of flow cytometry because that part is simply sitting at the machine and would only be relevant to readers and viewers with the exact same flow cytometer. However, the sample preparation is translatable to all potential readers and viewers who seek to use this technique.

2. Title Comment Regarding “Mononuclear Phagocytes”: this part is not well introduced in the introduction and not clearly described in the protocol.

Response: Mononuclear phagocytes are introduced on line 55-56 which are the first and second sentences of the introduction. We added “for Mononuclear Phagocytes” to 4.0 of the protocol so that the title of this highlighted section of the protocol now states: “Staining of Cell Suspension for Mononuclear Phagocytes” to add clarity.

3. Abstract Comment Regarding “fluorescence minus one control”: please bring out clarity on this.

Response: Fluorescence minus one controls (FMOs) are described in 5.6, 6.4, and Line 495-505 of the results, which explains how the FMO controls are used to draw positive gates are cells. Additionally, we changed the abstract from “drawing gates using FMOS” to “delineating positive gates using FMOs” to add clarity.

4. Introduction Comment Regarding “Mononuclear phagocytes, which are composed of monocytes, macrophages, and dendritic cells, have been implicated in the pathophysiology of multiple ophthalmic conditions including uveitis, diabetic retinopathy, and age-related macular degeneration (AMD).”: Please add citation.

Response: A citation has been added.

5. Introduction Comment Regarding “the laser-induced CNV model”: what is the significance of this?

Response: We added the following sentence: “Laser-induced CNV is the standard mouse model of neovascular AMD, which demonstrated the efficacy of current first line neovascular AMD therapy.” Line 163-164

6. General Comment of Protocol: We cannot film the notes section, I have removed the highlights. If anything needs to be filmed, please make an action step in imperative tense.

Response: All notes are no longer highlighted. We have confirmed that the highlighted section is 2.5 pages.

7. Comment in Note 1.1 Regarding “In our experience, systemic perfusion did not reduce the number of microglia, monocytes, macrophages, or dendritic cells detected in untreated whole eyes.”: Are there any citations supporting this claim? Please include.

Response: This section was a major concern of Reviewer 3. To address this concern, we subjected mice to laser and performed perfusion experiments to compare our macrophage numbers in both untreated and laser treated mice, and with and without systemic perfusion. Figure 5 shows this data which will be discussed in the results. The sentence now reads: “In our experience, systemic perfusion does not reduce the number of microglia, monocytes, macrophages, or dendritic cells detected in untreated or laser treated whole eyes (Fig 5).”

8. The editor added “Then cut the optic nerve with a pair of scissors” to section 1.3.

Response: Section 1.3 now reads, “Pull eye laterally until the optic nerve is the only remaining connection to detach the eye. The optic nerve often severs with tension, but a small scissor is sometimes necessary to cut the optic nerve.” The scissor is only needed sometimes. We removed the note below 1.3 since the new sentence clarifies both issues.

9. Comment in 3.2 regarding “flow buffer”: composition?

Response: The composition of flow buffer is described in the Table of Materials. To make this more clear, we capitalized “Flow buffer”.

10. Comment in 4.9 regarding “antibody staining solution”: All the antibodies are added together? Please somewhere bring out clarity on the choice of antibody for detection of mononuclear phagocytes with citation. why a particular choice was made to detect a particular cell type with citation.

Response: That is correct, all antibodies are added together in one solution or cocktail. We have amended the section to add clarity. 4.9 now reads, “Add 50 ul of antibody staining solution (see Table 1 for choice and amount of each antibody that is included in the solution) per 5 x 10^6 living cells directly to cells in Fc block and mix completely. Incubate for 30 minutes at 4 C.” Regarding the choice of antibodies, these are extensively discussed in the second paragraph of the introduction from Line 64-85 with citations.

11. Comment on 4.10 Note: This note describes action. Please convert it into numbered action step.

Response: This was a note because this step is optional. This step is now 4.11 and reads "OPTIONAL: After antibody staining, the samples can be fixed with 500 µl of 2% paraformaldehyde in flow buffer. Fix samples for 15 minutes at room temperature. Then, perform one wash as described in 4.10. Store fixed samples at 4 °C. Count beads should be added on day of flow cytometry data collection. Fixed samples should be run on flow cytometer in 1-2 days."

12. Comment of 5.3.5 Note: This can be moved to the results, instead.

Response: This section is now the first paragraph of the results.

13. Comment on representative results: Please describe the result with respect to your experiment, you performed an experiment, how did it help you to conclude what you wanted to and how is it in line with the title.

Response: The beginning paragraphs of the results section describe proper gating, FMO controls, and quantitative analysis. The experiment is described in the final paragraph. We lengthened, extended, and further highlighted the experiment to address this concern. The final paragraph of the results section now reads (Line 535-549): "Macrophages infiltrate the choroid after laser injury[11], and macrophage depletion reduces CNV area[14]. These older studies rely upon immunofluorescence imaging, which cannot reliably differentiate mononuclear phagocytes, or fewer markers for macrophage identification using flow cytometry. Macrophage heterogeneity is an emerging concept in innate immunology, where macrophages are capable of performing multiple functions depending upon their origin and tissue microenvironment[12,13]. We performed multi-parameter flow cytometry on untreated and laser treated mouse eyes on Day 3 after laser injury to identify mononuclear phagocytes and macrophage heterogeneity. Laser treatment increased $MHCII^-$, $CD11c^-$, and $CD11c^+$ macrophages by 7.0-25.6, 2.8-7.2, and 3.9-8.2 fold respectively (Fig 5A-C). Dendritic cell counts were also up-regulated 4.5-4.7-fold by laser (Fig 5F). Microglia and monocyte counts were not affected by laser treatment (Fig 5D-E). No significant differences were detected with or without systemic perfusion prior to enucleation. These results demonstrate increased macrophage populations and dendritic cells after laser injury with no change to microglia or monocytes. Furthermore, these data highlight how multi-parameter flow cytometry can detect macrophage heterogeneity."

14. Comment on figure and table legends: In the figures, please include percentage of cells obtained in each gating.

Response: We added the percent of parent to Figures 2-4 as requested.

15. Comment on discussion: please include critical steps in the protocol as well.

Response: Line 676-677 states, “The method of digestion, in section 2 of the protocol, is the most critical, while other steps in sections 3 - 5 have been used successfully on multiple tissue types”. This sentence is followed by a discussion of the critical step.

Reviewer #3

1. The lack of perfusion means that there is nothing to separate out circulating and intraocular immune cells. Based on this reviewer's experience there is a significant change specially in a healthy eye that has very little immune cells other than the microglial and maybe a few dendritic cells. The lack of difference the authors state with the laser wounded eyes may be because of the loss of the blood-ocular barrier that has allowed infiltration of cells from the periphery that overwhelm the cell number of intraocular immune cells. Still, there is no ability without perfusion for an analysis to focus on only the immune cell populations within the eye, resident or infiltrating.

Response: To address the reviewer’s concerns, we performed an experiment comparing untreated and laser treated eyes without systemic perfusion, to untreated and laser treated eyes with systemic perfusion of 15 ml ice cold HBSS via cardiac puncture directly after euthanasia and prior to enucleation. The results of the experiment are presented in Fig 5 and discussed in Line 535-548 of the results section. Laser treatment increased MHCII-, CD11c-, and CD11c+ macrophages both with and without systemic perfusion compared unlasered eyes. There was no statistical difference between no perfusion + laser and perfusion + laser-treated eyes. Dendritic cell counts were also up-regulated by laser both with and without perfusion. Microglia and monocyte counts were not affected by laser treatment.

Reviewer #4

Major Concerns:
1. The paper reads well, but another paper which compares inflammatory and resident myeloid populations in various models (EAU/EIU) and goes further wrt CNV (processing choroid and retina separately) is Flow cytometric analysis of inflammatory and resident myeloid populations in mouse ocular inflammatory models Sidath E.Liyanagea Peter J.Gardner JoanaRibeiro EnricoCristante Robert D.Sampson Ulrich F.O.Luhmanna Robin R.Ali James W.Bainbridge https://doi.org/10.1016/j.exer.2016.08.007. This should be cited.

Response: We have added a discussion of the key differences between our gating strategy and Liyanagea et al in Line 641-648 of the discussion, which states, “Liyanage et al recently reported a similar gating strategy to detect neutrophils, eosinophils, lymphocytes, DCs, macrophages, infiltrating macrophages, and monocytes. Our gating strategy primarily differs by the addition of CD64. Liyanage et al identifies DC as CD4-CD8-B220-CD11b+CD11c+ cells, and macrophages as CD4-CD8-B220-CD11b+CD11c-NK1.1-Ly6G- cells. We identify DC as CD4-CD8-B220-Ly6G-SiglecF-NK1.1-CD11b+CD11c+CD64- cells and macrophages as CD4-CD8-B220-Ly6G-SiglecF-NK1.1-CD11b+CD64+ cells. The use of CD64 to discriminate DC from macrophages is well established,

and this strategy allows us to identify macrophage heterogeneity, including CD11c+ macrophages.

2. In their approach: "retinal microglia can be differentiated from monocyte-derived macrophages by their dim levels of CD45 expression and high levels of Tmem119" but it is already well-recognised that microglia can upregulated CD45 expression during inflammation and that monocytes can downregulate CD45 during inflammation/activation (see Muller et al In J Cancer 2015, Cosenza-Nashat et al, Brain Pathology 2006, Sedgwick et al Journal of Imm 1998, and De Martinis et al Immunol Cell Biol 2004 for good papers on this). Therefore CD45 low population may not include microglia at-all, but also other cell types.

Response: This technique of discriminating microglia from macrophages is effective both in the retina and brain. This technique has been published by O'Koren et al (PMID: 26856416, PMID: 30850344) and Makinde et al (PMID: 32174913) both at steady state and in models of inflammation. We are currently preparing a manuscript using the Cx3cr1-CreER ; Rosa26-f-stop-f-GFP mouse. This mouse will label all Cx3cr1+ cells as GFP+, including monocytes, macrophages, and microglia. After a 4 weeks wash out period, the monocytes recycle and only tissue resident macrophages are GFP+. We performed laser 4-6 weeks after tamoxifen treatment and performed multi-parameter flow cytometry. We found that all CD45dim cells remained GFP+, demonstrating that they are microglia or tissue resident macrophages, and are not infiltrating immune cells. This data is beyond the scope of the Jove manuscript but is copied below for your review.

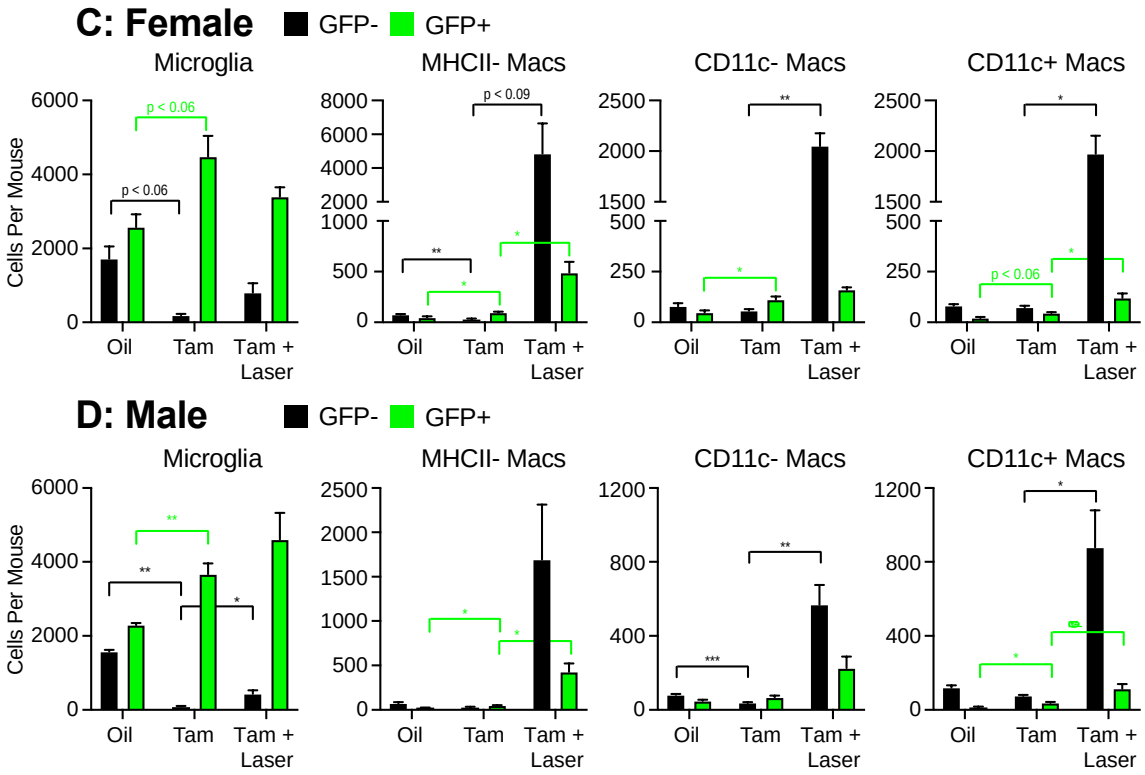

3. It is also becoming increasingly recognised that microglia lose their homeostatic transcript (Tmem119 is generally considered part of the homeostatic transcript) upon activation (e.g. Holtman et al Acta Neuropathologica Communications 2015, Bell et al Front Immunol 2020, Zrzavy et al Brain 2017, Sousa et al EMBO Biol 2018, O'Koren et al Immunity 2019, Krasemann et al Immunity 2017). Some Authors have already shown microglia can downregulate or lose expression of Tmem119 during perturbation (see Keren-Shaul et al Cell 2017). Therefore, it needs to be acknowledged that these markers for differentiation are not always fully specific for microglia depending on context as part of the introduction. It is currently unclear if changes in CD45/Tmem119 expression occurs during AMD and represents unknown/novel information. It seems like tmem119 was not used in the current study, and only simple pulling-apart of CD45 dim/high (of CD11b+ cells) was used to distinguish what they describe as microglia.

Response: A previous reviewer asked for us to include Tmem119 in our introduction regarding microglia. You are correct that we did not use Tmem119 in our protocol, just CD4-CD8-B220-SiglecF-NK1.1-Ly6G-CD11b+CD45dimCD64+ cells. We agree that many aspects of microglia biology remain unknown and uninvestigated. We have added “Upon microglia activation, however, CD45 can be up-regulated and Tmem119 may be down-regulated, demonstrating the complexity of microglia biology and this is likely relevant in both AMD and its mouse model” of the introduction to Line 80-82 to satisfy this concern.

Minor Concerns:
1. It might be nice for the data from the empirical study to be included as a supplementary? (optional)

Response: In the discussion (Line 682-688), we have added more detail to our iterative digestion optimization. It now reads, “We arrived at our digestion conditions through an iterative method that involved: (1) testing of chemical digestion method (Collagenase D vs digestion enzyme), (2) determination of length of chemical digestion (30, 60, and 90 minutes), and (3) addition of mechanical digestion (none, once, twice, three times). At each step we judged the success of the digestion conditions by cell viability and number of $CD45^{Hi}CD64^{+}$ (infiltrating macrophages) cells. We found that digestion enzyme (see Supplementary Table of Materials) recovered more live cells than Collagenase D, and attempting half of the digestion enzyme concentration resulted in fewer infiltrating macrophages. Next, 60 minutes of chemical digestion with mechanical digestion nearly doubled the infiltrating macrophage populations. Three mechanical digestions was optimal with 25-30% live cells of singlets and the most infiltrating macrophage populations. Finally, faster digestion conditions caused severe loss of both live cells and macrophages.”

2. Regarding 2.6: "gentle rotation" is not described with enough detail for another researcher to replicate. Is this at room temperature, chilled, and what speed/rpm?

Response: We have changed 2.6 to read: “Place dissociation tube inverted onto electronic dissociator and run cycle “m_brain_03_01”, consisting of 1 min unidirectional rotation at 200 rpm at room temperature, which is a pre-loaded program. Ensure all tissue is at the bottom of the dissociation tube in contact with digestion buffer for this and all remaining steps.”

3. Regarding 2.7: what speed?

Response: The speed is 200 rpm. This has been added to 2.7.

4. No indication of % cell viability (Figure 2) using their iteratively determined digestion conditions. What would be helpful is to include this in relation to their iterative method used to determine the final conditions?

Response: Figures 2-4 now includes the percentages of parent, which include % Live Cells of Singlets. Additionally, in the discussion (Line 682-688), we have added more detail to our iterative digestion optimization. It now reads, “We arrived at our digestion conditions through an iterative method that involved: (1) testing of chemical digestion method (Collagenase D vs digestion enzyme), (2) determination of length of chemical digestion (30, 60, and 90 minutes), and (3) addition of mechanical digestion (none, once, twice, three times). At each step we judged the success of the digestion conditions by cell viability and number of $CD45^{Hi}CD64^{+}$ (infiltrating macrophages) cells. We found that digestion enzyme (see Supplementary Table of Materials) recovered more live cells than Collagenase D, and attempting half of the digestion enzyme concentration resulted in fewer infiltrating macrophages. Next, 60 minutes of chemical digestion with mechanical digestion nearly doubled the infiltrating macrophage populations. Three mechanical digestions was optimal with 25-30% live cells of singlets and the most infiltrating macrophage populations. Finally, faster digestion conditions caused severe loss of both live cells and macrophages.”